Radiology: Imaging Cancer

ORIGINAL RESEARCH

Prediction of Macrotrabecular-Massive Hepatocellular Carcinoma and Associated Prognosis Using Contrast-enhanced US and Clinical Features

Jiapeng Wu, MD[*1,2,4] • *Sisi Liu, MD*[*3,4] • *Yiqiong Zhang, MD*[4] • *WenZhen Ding, MD*[2,4] • *Qinxian Zhao, MD*[2,4] • *Yuling Wang, MD*[2,4] • *Fan Xiao, MD*[2,4] • *Xiaoling Yu, MD*[4] • *Xiaoyan Xie, MD*[5] • *Shuhong Liu, MD*[6] • *Jingmin Zhao, MD*[6] • *Jintang Liao, MD*[7] • *Jie Yu, MD*[2,4] • *Ping Liang, MD*[1,2,4]

* J.W. and Sisi Liu contributed equally to this work.

Author affiliations, funding, and conflicts of interest are listed at the end of this article.

Radiology: Imaging Cancer 2025; 7(4):e240419 • https://doi.org/10.1148/rycan.240419 • Content codes: GU OI US

Purpose: To develop a combined contrast-enhanced US (CEUS) clinical model for the prediction of macrotrabecular-massive hepatocellular carcinoma (MTM HCC) and evaluate its diagnostic and prognostic values.

Materials and Methods: This secondary analysis of a prospective multicenter study (ClinicalTrials.gov: NCT04682886) included participants from three independent cohorts who underwent CEUS and surgical resection for HCC between January 2017 and December 2022. Two radiologists independently reviewed CEUS data, and the interreader agreement was evaluated. Logistic regression was performed using the training cohort to determine the predictors associated with MTM HCC, while the validation cohort was used to evaluate the diagnostic and prognostic values of the predictors.

Results: A total of 387 participants (mean age, 55.09 years ± 10.33 [SD]; 342 male) were included. Four clinical and CEUS features were associated with MTM HCC: early washout (before 60 seconds) (odds ratio [OR]: 8.82 [95% CI: 4.22, 18.64], $P < .001$), hypoenhancing component (OR: 4.03 [95% CI: 1.78, 9.49], $P < .001$), tumor size (OR: 1.28 [95% CI: 1.04, 1.59], $P = .02$), and serum α-fetoprotein level greater than 100 ng/mL (OR: 3.01 [95% CI: 1.41, 6.63], $P = .004$). The combined predictive model yielded an area under the receiver operating characteristic curve of 0.89 (95% CI: 0.85, 0.93) in the training cohort and 0.81 (95% CI: 0.73, 0.89) in the validation cohort. The model also achieved a negative predictive value of 94.2% (147 of 156) in the training cohort and 88.0% (66 of 75) in the validation cohort, with high prognostic accuracy for overall survival (hazard ratio: 2.26 [95% CI: 1.07, 4.79], $P = .03$).

Conclusion: The combined CEUS-clinical predictive model could be used to characterize the MTM HCC subtype and determine prognosis.

Clinical trial registration no. NCT04682886

Supplemental material is available for this article.

Hepatocellular carcinoma (HCC) is the third leading cause of cancer-related deaths worldwide (1,2). With approximately 70.0% of patients experiencing tumor recurrence after resection, the overall outcomes of HCC remain unsatisfactory (3). Owing to a high degree of molecular and histologic heterogeneity (4), advanced histopathologic architectural patterns have been differentiated to further classify HCC (5,6). Among these patterns, macrotrabecular-massive (MTM) HCC exhibits an aggressive biologic behavior, rapid tumor progression, and an elevated risk of recurrence (5–9). This subtype was introduced in the fifth edition of the World Health Organization Classification of Tumors (10). Approximately 10.0%–38.2% of HCCs are classified as MTM HCC; however, this proportion is higher in regions with increased rates of hepatitis B virus (HBV) infection (4,11,12).

Despite the severity of the MTM HCC subtype, its diagnosis can only be confirmed through a histopathologic review performed after resection (7); therefore, the histopathologic information is not available for patients undergoing treatments such as transcatheter arterial chemoembolization and ablation (13). Additionally, heterogeneity in HCC subtypes might influence treatment outcomes. Lin et al (14) reported that lipiodol deposition rate was significantly higher in patients with MTM HCC undergoing conventional transarterial chemoembolization compared with those with non-MTM HCC subtypes, while Ziol et al (7) revealed that MTM HCC is associated with frequent recurrence after radiofrequency ablation for HCC. Woo et al (15) reported that patients with MTM HCC have a higher proportion of lung metastasis. Therefore, having a preoperative diagnosis of MTM HCC can aid in treatment decision-making, such as when deciding between wide-margin resection and anatomic hepatectomy. An accurate preoperative diagnosis may also support recommendations for a shorter surveillance follow-up in patients undergoing nonsurgical treatments.

Several studies have reported associations between imaging features and MTM HCC. Mulé et al (9) found that substantial necrosis at MRI could help to identify MTM HCC. Feng et al (11) found that intratumoral necrosis and hemorrhage observed at CT were independent predictors of MTM HCC, and Rhee et al (16) demonstrated that the absence of a hypovascular component during the arterial phase had a high

Abbreviations

AFP = α-fetoprotein, APHE = arterial phase hyperenhancement, AUC = area under the receiver operating characteristic curve, CEUS = contrast-enhanced US, HBV = hepatitis B virus, HCC = hepatocellular carcinoma, HR = hazard ratio, MTM = macrotrabecular massive, NPV = negative predictive value, OR = odds ratio, OS = overall survival

Summary

A preoperative multivariable model including contrast-enhanced US and clinical features was predictive of macrotrabecular-massive hepatocellular carcinoma, which was associated with poor patient prognosis.

Key Points

- In 387 individuals with hepatocellular carcinoma (HCC), early washout (odds ratio [OR]: 8.82, $P < .001$) and a hypoenhancing component at contrast-enhanced US (OR: 4.03, $P < .001$), tumor size (OR: 1.28, $P = .02$), and serum α-fetoprotein level (OR: 3.01, $P = .004$) were independently associated with the macrotrabecular-massive (MTM) HCC subtype.
- A preoperative logistic regression model combining these CEUS and clinical features predicted MTM HCC with areas under the receiver operating characteristic curves of 0.81 and 0.89 in the training and validation cohorts, respectively.
- Prediction of MTM HCC by the model was associated with worse overall survival (hazard ratio: 2.26, $P = .03$).

Keywords

Molecular Imaging–Angiogenesis, Ultrasound-Contrast, Liver, Macrotrabecular-Massive Hepatocellular Carcinoma, Contrast-enhanced US

negative predictive value (NPV) for MTM HCC. However, compared with CT and MRI, contrast-enhanced US (CEUS) offers several advantages in the real-time observation of tumor perfusion, allowing for dynamic characterization of the perfusion of tumors and the liver and acting as a blood pool agent, which may reflect the distinct microvascular structure of the tumor and its infusion status.

As there is a paucity of studies focused on the CEUS features of MTM HCC (17), we aimed to evaluate these features, develop a combined CEUS-clinical MTM HCC predictive model, and evaluate its diagnostic and prognostic values.

Materials and Methods

This retrospective study was a secondary analysis of a prospective multicenter study (ClinicalTrials.gov: NCT04682886) that included participants enrolled from a national Chinese registry of liver lesion US studies and was approved by the institutional review board of the People's Liberation Army General Hospital (Beijing, China; approval no.: S2017-046-03). The requirement for informed consent was waived owing to the retrospective nature of the study.

Study Design and Participants

The following data were retrospectively collected from a Chinese multicenter database: clinical characteristics, laboratory results, and CEUS data. The training cohort was used to identify the optimal clinical and CEUS features for establishing a diagnosis of MTM HCC, and the validation cohort was used to validate the robustness of the CEUS and clinical features. The training cohort comprised 251 participants who underwent resection for primary HCC at any of the three institutions (Fifth Medical Center of People's Liberation Army General Hospital, Beijing, China; First Medical Center of People's Liberation Army General Hospital, Beijing, China; and First Affiliated Hospital, Sun Yat-sen University, Guangzhou, China) between January 2022 and December 2022, while the validation cohort consisted of 136 participants who underwent resection at a fourth institution (Xiangya Hospital Central South University, Changsha, China) between January 2017 and December 2022. The inclusion criteria for both cohorts were as follows: *(a)* histopathologically proven HCC, *(b)* surgical resection as the first-line treatment, and *(c)* preoperative CEUS data being available. The exclusion criteria were as follows: *(a)* poor CEUS quality owing to fatty liver or shelter from the lung, *(b)* poor histologic slide quality, and *(c)* extended period (>3 months) between the most recent resection and CEUS. Participants underwent regular postresection follow-up using CT and/or MRI every 3–6 months to evaluate their recurrence-free survival—the length of time a participant survives without any local or distant tumor recurrence or death.

CEUS Acquisition

CEUS cine clips aimed at diagnosing liver lesions, using SonoVue (Bracco Imaging) as a contrast agent, were obtained from a multicenter cohort. For participants with multiple liver lesions, the largest lesion was selected for CEUS evaluation. A 2.4-mL intravenous bolus injection of the contrast agent was administered through the cubital vein, followed by a 5-mL saline flush. The timer was set at the same time as contrast agent administration, and CEUS cine clips were obtained at the following time intervals: 0–2 minutes, 3 minutes to 3 minutes 10 seconds, 4 minutes to 4 minutes 10 seconds, and 5 minutes to 5 minutes 10 seconds. All CEUS cine clips and their corresponding clinical characteristics were stored and uploaded to a database dedicated to this study *(http://www.usliver.org/home.html)*. For detailed information about the CEUS examination protocol and data storage, please refer to Appendix S1.

Image Analysis

Two board-certified radiologists (Sisi Liu and J.W., with 10 and 7 years of experience in liver CEUS examinations, respectively) independently reviewed all CEUS cine clips. Both radiologists were blinded to the pathologic diagnosis and clinical characteristics, and in instances where the radiologists disagreed, a third radiologist (J.Y., with >20 years of experience in liver CEUS examinations) provided the definitive evaluation, and the third radiologist's judgment was considered final without further arbitration. Interobserver agreement was assessed following the independent review. Various CEUS features were evaluated, including arterial phase hyperenhancement (APHE), rim APHE, washout, early washout, marked washout, intratumoral artery, necrosis, hypoenhancing component, and CEUS Liver Imaging Reporting and Data System version 2017 category (for participants at high risk). Early washout was defined as the onset of washout within 60 seconds from the injection of the contrast agent, while marked washout appeared black or punched out within 2 minutes,

according to CEUS Liver Imaging Reporting and Data System version 2017 (18). The hypoenhancing component was defined as the inhomogeneous enhancement of the tumor with an approximate nonenhancing region (>20.0%) in the early arterial phase (10–20 seconds), with contrast agent inflow occurring gradually between 30 and 45 seconds and a persistent hypoenhancing appearance. Washout in the portal and/or late phase may or may not be present, while the presence of contrast agent infusion within the tumor was the main feature for differentiating between tumor and necrosis, which was identified as a continuous nonenhancing region observed during all three phases. The intratumoral artery was defined as enhancing vessels within the tumor during the arterial phase, as previously described (16). The details of the CEUS features are summarized in Table S1.

Histopathologic Analysis

The following histologic information was obtained from each pathology report: number of lesions, tumor size, Edmonson-Steiner differentiation grade, and microvascular invasion. In cases of multiple lesions, histopathologic analysis was performed on the largest lesion, and each evaluation was conducted by four experienced pathologists, each with at least 15 years of experience, in each cohort. MTM HCC was defined by a predominantly macrotrabecular architectural pattern (>50.0% of the tumor area, with trabeculae > six cells thick) with hematoxylin-eosin staining, as previously reported (4,16,19).

Statistical Analysis

Statistical analyses were performed using R software (version 4.2.1; R Foundation for Statistical Computing, *http://www.r-project.org*). Continuous variables are presented as means ± SDs, while categorical variables are presented as frequencies and percentages. χ^2 and Fisher tests were used for comparing clinical characteristics between the non-MTM and MTM groups, whereas Student *t* test was used for continuous variables, which were first assessed for linearity in the logit scale using Box-Tidwell tests. Univariable logistic regression with a lenient threshold ($P < .1$) was used for the initial screening, after which a multivariable model was constructed using backward stepwise elimination based on the Akaike information criterion. Multicollinearity among predictors was assessed using the variance inflation factor and tolerance values. Interobserver agreement was assessed using the Cohen κ coefficient, with coefficients ranging from 0 to 1 indicating poor to excellent agreement, respectively. The performance of the MTM HCC prediction model was evaluated using receiver operating characteristic curves, areas under the receiver operating characteristic curves (AUCs), sensitivity, specificity, and NPV. The calibration curve was evaluated using the Brier score for overall prediction accuracy and Hosmer-Lemeshow test for goodness of fit. The survival probabilities were estimated using the Kaplan-Meier method and compared using log-rank test. Univariable Cox regression was used for the initial screening of the predictors of overall survival (OS, $P < .10$), while multivariable Cox regression analysis using backward stepwise elimination-based Akaike information criterion was used to determine the potential predictors of OS from all preoperative parameters. Proportional hazards assumptions were evaluated using Schoenfeld residuals for all covariates. A two-sided *P* value less than .05 was considered statistically significant for all analyses.

Results

Participant Characteristics

A total of 491 participants underwent resection for HCC during the study period; however, 104 were excluded for various reasons, including treatment before resection ($n = 38$), missing or incomplete CEUS cine clips ($n = 25$), poor-quality pathologic slides ($n = 15$), poor-quality CEUS cine clips due to fatty liver or shelter from the lung ($n = 16$), and interval longer than 3 months between treatment and CEUS ($n = 10$, Fig 1). The participants were divided into training ($n = 251$; mean age, 55.7 years ± 9.5; 218 male [86.9%], 33 female [13.1%]) and validation ($n = 136$; mean age, 54.0 years ± 11.6; 124 male [91.2%], 12 female [8.8%]) cohorts. The pathologic characteristics of both cohorts are shown in Table 1. In the training and validation cohorts, 27.1% (68 of 251) and 35.3% (48 of 136) of the participants were diagnosed with MTM HCC, respectively. Additionally, most participants in both cohorts had HBV infection as the primary cause (training cohort: 203 of 251, 80.9%; validation cohort: 126 of 136, 92.6%), followed by cirrhosis (training cohort: 163 of 251, 64.9%; validation cohort: 104 of 136, 76.5%). A Barcelona Clinic Liver Cancer stage of 0–A was common in the training (215 of 251, 85.7%) and validation (100 of 136, 73.5%) cohorts.

Clinical and CEUS Features of MTM HCC

Table 2 summarizes the clinical and CEUS features of MTM and non-MTM HCC. In terms of CEUS features, MTM HCC cases (Fig 2) exhibited a higher frequency of early washout than did non-MTM HCC cases (Fig 3) in both the training (72.1% vs 12.0%, $P < .001$) and validation (64.6% vs 22.7%, $P < .001$) cohorts. Additionally, MTM HCC cases had a higher prevalence of hypoenhancing components than did non-MTM HCC cases in both the training (50.0% vs 19.1%, $P < .001$) and validation (60.4% vs 28.4%, $P = .001$) cohorts. However, we found no evidence of differences between the MTM and non-MTM HCC cases in terms of rim APHE, washout, marked washout, necrosis, and intratumoral artery (all $P \geq .05$) in either cohort. The interobserver agreements for CEUS features showed moderate to excellent agreement (κ = 0.61–0.84, Table S2). In both the training and validation cohorts, MTM HCC exhibited a larger tumor size than did non-MTM HCC ($P = .03$ and .005, respectively). Furthermore, in both cohorts, MTM HCC showed a higher prevalence of microvascular invasion than did non-MTM HCC (training cohort: 72.1% vs 50.3%, $P = .009$; validation cohort: 66.7% vs 38.6%, $P = .003$). However, we found no evidence of a difference in the number of tumors between MTM and non-MTM HCC in either cohort ($P > .05$).

Development and Validation of a Predictive Model for MTM HCC

The independent predictors of MTM HCC, as determined with multivariable logistic regression analysis, were early

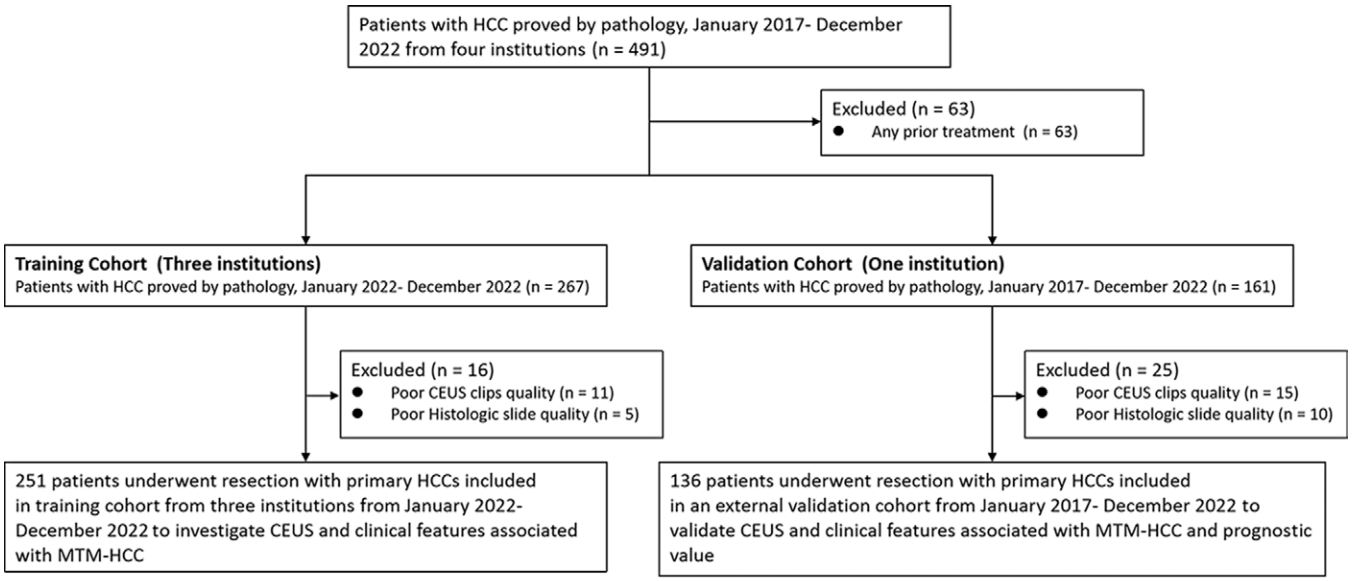

Figure 1: Flow diagram. CEUS = contrast-enhanced US, HCC = hepatocellular carcinoma, MTM = macrotrabecular massive.

Table 1: Clinical and Pathologic Characteristics of Participants in Training and Validation Cohorts

Variable	Training Cohort (*n* = 251)	Validation Cohort (*n* = 136)	*P* Value
Sex			.27
Male	218 (86.9)	124 (91.2)	
Female	33 (13.1)	12 (8.8)	
Age (y)	55.7 ± 9.5	54.0 ± 11.6	.15
Cause			<.001
Alcoholism	1 (0.4)	5 (3.7)	
HBV	203 (80.9)	126 (92.6)	
HCV	5 (2.0)	1 (0.7)	
Other	3 (1.2)	0 (0)	
Unknown	39 (15.5)	4 (2.9)	
Cirrhosis	163 (64.9)	104 (76.5)	.03
Serum AFP level ≥ 100 ng/mL	96 (38.2)	78 (57.4)	<.001
PLT count (10^9/L)	170.0 ± 67.4	154.0 ± 82.3	.05
ALB level (g/L)	40.7 ± 4.3	40.0 ± 4.43	
TBIL level (μmol/L)	13.5 ± 5.1	12.8 ± 5.11	
DBIL level (μmol/L)	6.0 ± 3.1	6.3 ± 2.9	
Microvascular invasion	141 (56.2)	66 (48.5)	.15
Macrovascular invasion	28 (11.2)	16 (11.8)	.99
Tumor size (cm)	3.7 ± 1.9	6.2 ± 3.4	<.001
BCLC stage (B–C)	36 (14.3)	36 (26.5)	.005
Multiple lesions	21 (8.4)	31 (22.8)	<.001
MTM HCC	68 (27.1)	48 (35.3)	.12

Note.—Data are numbers of participants, with percentages in parentheses, or means ± SDs. AFP = α-fetoprotein, ALB = albumin, BCLC = Barcelona Clinic Liver Cancer, DBIL = direct bilirubin, HBV = hepatitis B virus, HCC = hepatocellular carcinoma, HCV = hepatitis C virus, MTM = macrotrabecular massive, PLT = platelet, TBIL = total bilirubin.

Table 2: Clinical and Pathologic Characteristics of Participants according to MTM HCC in Training Cohort and Validation Cohort

Variable	Training Cohort			Validation Cohort		
	Non-MTM (n = 183)	MTM (n = 68)	P Value	Non-MTM (n = 88)	MTM (n = 48)	P Value
Clinical characteristic						
Sex						
Male	156 (85.2)	62 (91.2)	.30	79 (89.8)	45 (93.8)	.54
Female	27 (14.8)	6 (8.8)		9 (10.2)	3 (6.2)	
Age (y)	55.9 ± 9.4	54.1 ± 9.9	.19	56.2 ± 11.1	50.0 ± 11.6	.003*
Cause			.16			.77
Alcoholism	1 (0.5)	0 (0)		4 (4.6)	1 (2.1)	
HBV	146 (79.8)	57 (83.8)		81 (92.0)	45 (93.8)	
HCV	2 (1.1)	3 (4.4)		1 (1.1)	0 (0)	
Other	3 (1.6)	0 (0)		0 (0)	0 (0)	
Without	31 (16.9)	8 (11.8)		2 (2.3)	2 (4.2)	
Cirrhosis	119 (65.0)	44 (64.7)	.99	69 (78.4)	35 (72.9)	.61
Serum AFP level ≥ 100 ng/mL	58 (31.7)	38 (55.9)	<.001*	43 (48.9)	35 (72.9)	.01*
PLT count (10^9/L)	167 ± 71.3	178 ± 54.7	.28	149.0 ± 80.9	162.0 ± 85.2	.41
ALB level (g/L)	40.8 ± 4.4	40.5 ± 4.2	.64	39.6 ± 4.3	40.7 ± 4.6	.22
TBIL level (μmol/L)	13.4 ± 5.3	13.7 ± 4.8	.69	13.3 ± 5.6	12.0 ± 4.0	.13
DBIL level (μmol/L)	6.1 ± 3.0	5.6 ± 3.4	.38	6.3 ± 2.8	6.2 ± 3.2	.77
Microvascular invasion	92 (50.3)	49 (72.1)	.009*	34 (38.6)	32 (66.7)	.003*
Macrovascular invasion	22 (12.0)	6 (8.8)	.62	9 (10.2)	7 (14.6)	.64
Tumor size (cm)	3.5 ± 1.7	4.2 ± 2.3	.03*	5.5 ± 3.1	7.3 ± 3.6	.005*
BCLC stage (B–C)	28 (15.3)	8 (11.8)	.61	22 (25)	14 (29.2)	.59
Multiple lesions	17 (9.3)	4 (5.9)	.18	21 (23.8)	10 (20.8)	.99
CEUS features						
Rim APHE	8 (4.4)	3 (4.4)	.99	5 (5.7)	3 (6.3)	.99
Washout	165 (90.2)	67 (98.5)	.05	78 (88.6)	44 (91.7)	.77
Early washout	22 (12.0)	49 (72.1)	<.001*	20 (22.7)	31 (64.6)	<.001*
Marked washout	13 (7.1)	11 (16.2)	.05	10(11.4)	10 (20.8)	.22
Necrosis	24 (13.1)	6 (8.8)	.48	44 (50.0)	29 (60.4)	.32
Intratumoral artery	78 (42.6)	32 (47.1)	.63	57 (64.8)	36 (75.0)	.30
Hypoenhancing component	35 (19.1)	34 (50.0)	<.001*	25 (28.4)	29 (60.4)	.001*
CEUS LI-RADS category†			<.001*			<.001*
LR-3	4 (2.4)	1 (1.6)		0 (0)	0 (0)	
LR-4	12 (7.2)	0 (0)		7 (8.2)	5 (10.6)	
LR-5	109 (65.7)	16 (25.8)		50 (58.8)	11 (23.4)	
LR-M	36 (21.7)	44(71.0)		22 (25.9)	25 (53.2)	
LR-TIV	5 (3.0)	1 (1.6)		6 (7.1)	6 (12.8)	

Note.—Data are numbers of participants, with percentages in parentheses, or means ± SDs. AFP = α-fetoprotein, ALB = albumin, APHE = arterial phase hyperenhancement, BCLC = Barcelona Clinic Liver Cancer, CEUS = contrast-enhanced US, DBIL = direct bilirubin, HBV = hepatitis B virus, HCC = hepatocellular carcinoma, HCV = hepatitis C virus, LI-RADS = Liver Imaging Reporting and Data System, MTM = macrotrabecular massive, PLT = platelet, TBIL = total bilirubin.

* Statistically significant (P < .05).

† Only for participants at high risk according to CEUS LI-RADS version 2017, that is, participants with cirrhosis, HBV infection, or prior HCC (228 of 251 participants in training cohort and 132 of 136 participants in validation cohort).

washout (odds ratio [OR]: 8.82 [95% CI: 4.22, 18.64], P < .001), hypoenhancing component (OR: 4.03 [95% CI: 1.78, 9.49], P < .001), tumor size (OR: 1.28 [95% CI: 1.04, 1.59], P = .02), and α-fetoprotein (AFP) level (OR: 3.01 [95% CI: 1.41, 6.63], P = .004) (Table 3). All the variables demonstrated acceptable collinearity (variance inflation factor < 1.28, tolerance > 0.78), which was well below the recommended thresholds (variance inflation factor > 5, tolerance < 0.2).

A prediction model for MTM HCC was developed based on the aforementioned features, the details of which are

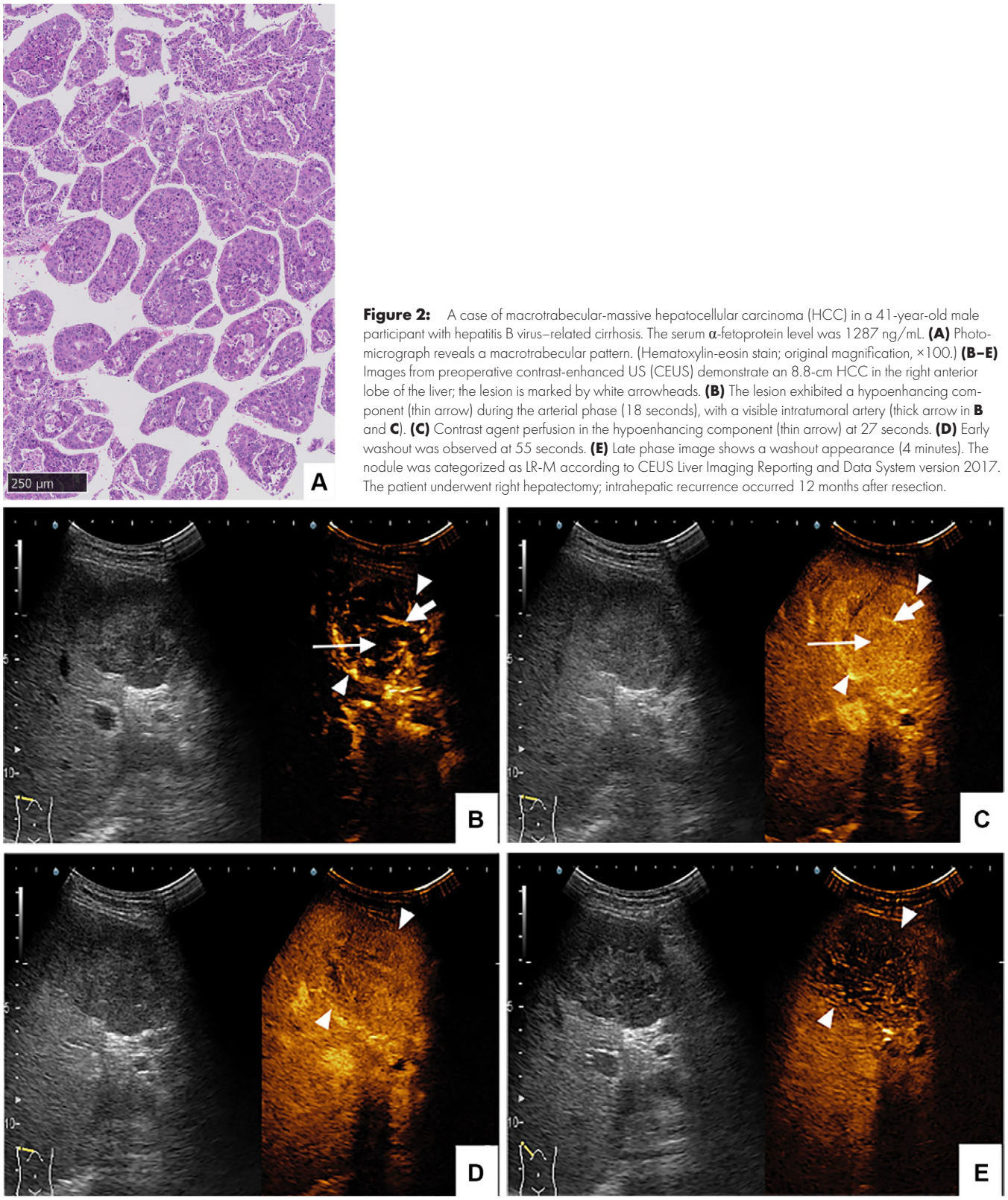

Figure 2: A case of macrotrabecular-massive hepatocellular carcinoma (HCC) in a 41-year-old male participant with hepatitis B virus–related cirrhosis. The serum α-fetoprotein level was 1287 ng/mL. **(A)** Photomicrograph reveals a macrotrabecular pattern. (Hematoxylin-eosin stain; original magnification, ×100.) **(B–E)** Images from preoperative contrast-enhanced US (CEUS) demonstrate an 8.8-cm HCC in the right anterior lobe of the liver; the lesion is marked by white arrowheads. **(B)** The lesion exhibited a hypoenhancing component (thin arrow) during the arterial phase (18 seconds), with a visible intratumoral artery (thick arrow in **B** and **C**). **(C)** Contrast agent perfusion in the hypoenhancing component (thin arrow) at 27 seconds. **(D)** Early washout was observed at 55 seconds. **(E)** Late phase image shows a washout appearance (4 minutes). The nodule was categorized as LR-M according to CEUS Liver Imaging Reporting and Data System version 2017. The patient underwent right hepatectomy; intrahepatic recurrence occurred 12 months after resection.

summarized in Appendix S2. The combined model, which incorporated all four CEUS and clinical features, achieved an AUC of 0.89 (95% CI: 0.85, 0.93) in the training cohort and 0.81 (95% CI: 0.73, 0.89) in the validation cohort. The nomogram of the combined model in the training and validation cohorts is shown in Figure 4A. Additionally, the calibration curves for the training and validation cohorts are shown in Figure 4B. The Brier score was 0.12 (95% CI: 0.08, 0.14) in the training and 0.17 (95% CI: 0.13, 0.20) in the validation cohort. The Hosmer-Lemeshow test showed no evidence of a lack of fit (training cohort: $P = .72$ vs validation cohort: $P = .86$). Furthermore, the combined model demonstrated the highest NPV for MTM HCC in both the training (94.2% [95% CI: 90.6, 97.9]) and validation (88.0% [95%

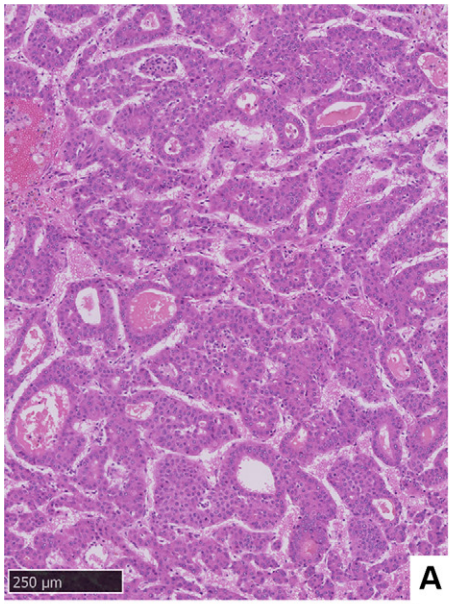

Figure 3: A case of non–macrotrabecular-massive hepatocellular carcinoma (HCC) in a 51-year-old male participant with hepatitis B virus–related cirrhosis and pseudoglandular HCC. The serum α-fetoprotein level was 2.4 ng/mL. **(A)** Photomicrograph reveals a pseudoglandular pattern. (Hematoxylin-eosin stain; original magnification, ×100.) **(B–E)** Images from preoperative contrast-enhanced US (CEUS) demonstrate a 5.0-cm HCC in the right anterior lobe of the liver; the lesion is marked by white arrowheads. **(B)** The lesion exhibited a homogeneous hyperenhancement in the arterial phase without necrosis (15 seconds). **(C)** No washout was observed at 60 seconds. **(D)** Mild washout was observed at 192 seconds. **(E)** Late phase image shows a washout appearance (249 seconds). The nodule was categorized as LR-5 according to CEUS Liver Imaging Reporting and Data System version 2017. The participant underwent right hepatectomy without recurrence during 36 months of follow-up.

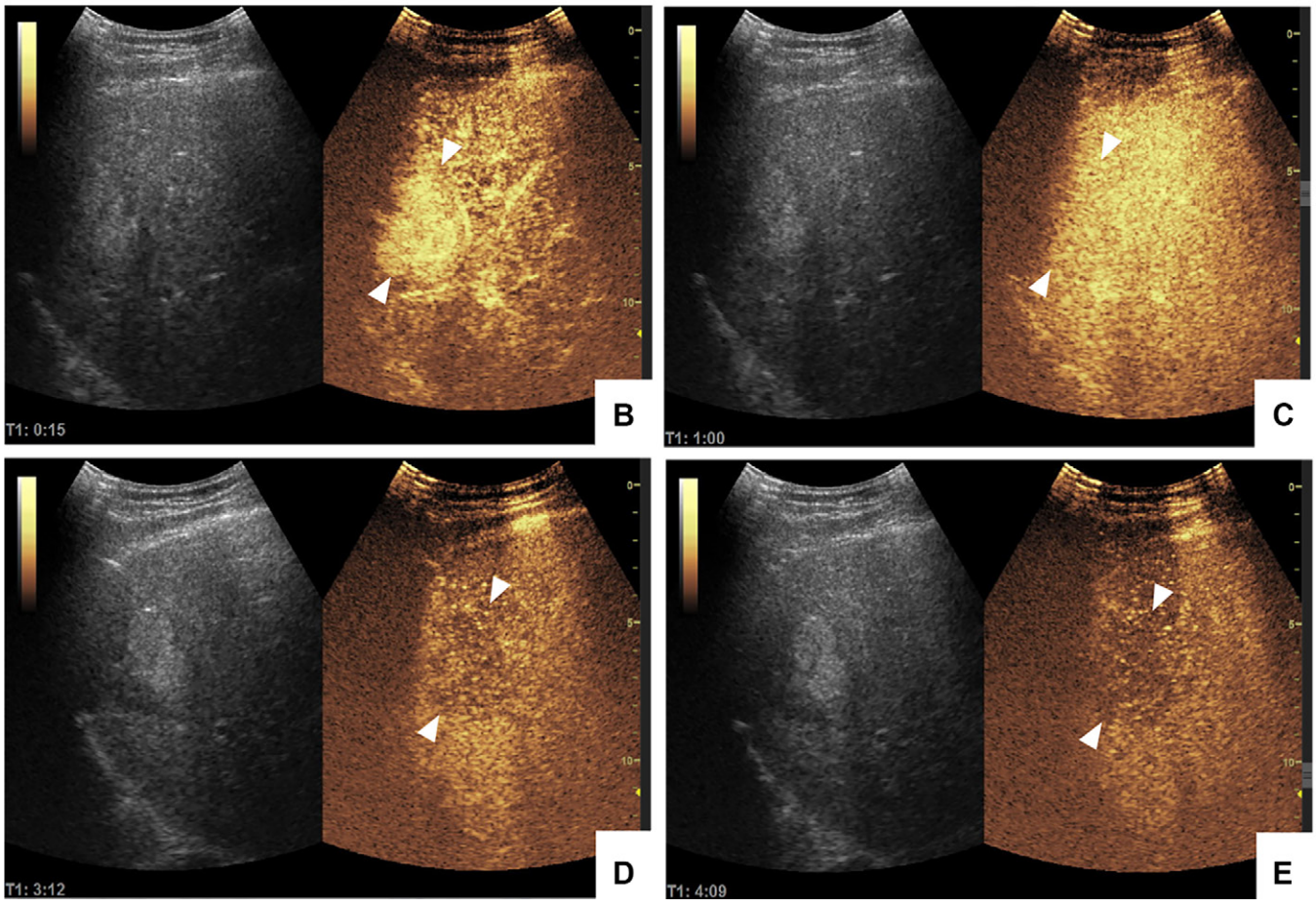

CI: 80.6, 95.4]) cohorts. The diagnostic performance of the model is shown in Table S3, while the distribution of predictive values among the participants is shown in Figure 4C. In the validation cohort, the median follow-up duration was 26.5 months (range, 1–63.0 months). The OS rate in all participants was 95.4%, 62.9%, and 50.1% at 1, 3, and 5 years, respectively. Based on the combined model, we divided the participants into two risk groups in the validation cohort using the ideal cutoff established from the training cohort. The 1-, 3-, and 5-year OS rates were 98.5%, 75.3%, and 65.7%, respectively, in the low-risk group and 87.7%, 44.8%, and 29.7%, respectively, in the high-risk group ($P < .001$). The 1-, 3-, and 5-year recurrence-free survival rates in the low-risk group were 91.3%, 63.0%, and 40.7%, respectively, which were better than those in the high-risk group (84.4%, 45.5%, and 30.1%, respectively; $P = .03$) (Fig 4D). Proportional hazards assumptions were evaluated using Schoenfeld residuals for all covariates, with no variables violating the

Table 3: Clinical and CEUS Features of MTM HCC by Logistic Regression Analysis

Variable	Univariable OR	*P* Value	Multivariable OR	*P* Value
Clinical characteristic				
Sex (male vs female)	1.92 (0.74, 5.10)	.21	...	...
Age	0.99 (0.95, 1.02)	.18	...	...
Serum AFP level ≥ 100 ng/mL	2.52 (1.44, 4.54)	.002*	3.01 (1.41, 6.63)	.004*
PLT count	0.99 (0.95, 1.02)	.33	...	...
ALB level	0.98 (0.92, 1.05)	.64	...	...
TBIL level	1.01 (0.95, 1.07)	.70	...	...
DBIL level	0.95 (0.86, 1.05)	.35	...	...
Tumor size	1.18 (1.02, 1.37)	.02*	1.28 (1.04, 1.59)	.02*
BCLC stage (B–C)	0.74 (0.29, 1.84)	.58	...	...
Multiple lesions	3.21 (0.77, 14.22)	.13	...	...
CEUS features				
Rim APHE	0.70 (0.21, 3.31)	.65	...	...
Washout	6.10 (0.86, 47.81)	.08*	...	...
Early washout	7.83 (4.06, 14.95)	<.001*	8.82 (4.22, 18.64)	<.001*
Marked washout	2.35 (0.82, 6.64)	.14	...	...
Necrosis	0.95 (0.42, 2.35)	.94	...	...
Intratumoral artery	1.65 (0.95, 2.91)	.09*	...	...
Hypoenhancing component	4.23 (2.33, 7.77)	<.001*	4.03 (1.78, 9.49)	<.001*

Note.—Data in parentheses are 95% CIs. AFP = α-fetoprotein, ALB = albumin, APHE = arterial phase hyperenhancement, BCLC = Barcelona Clinic Liver Cancer, CEUS = contrast-enhanced US, DBIL = direct bilirubin, HCC = hepatocellular carcinoma, MTM = macrotrabecular massive, OR = odds ratio, PLT = platelet, TBIL = total bilirubin.
* Statistically significant ($P < .1$)

assumption ($P > .05$). In multivariable Cox regression analysis for OS, albumin level (hazard ratio [HR]: 0.90 [95% CI: 0.83, 0.98], $P = .01$), tumor size (HR: 1.16 [95% CI: 1.06, 1.27], $P = .001$), multiple lesions (HR: 1.99 [95% CI: 1.00, 3.96], $P = .048$), and predicted MTM HCC (HR : 2.26 [95% CI: 1.07, 4.79], $P = .03$) were independent predictors for OS, and the concordance index was 0.78 (95% CI: 0.72, 0.84; Table 4).

Discussion

Various histopathologic architectural patterns of HCC have been described over the last few decades, among which MTM HCC has been characterized as having an unfavorable prognosis (6–8); however, not many studies have focused on the specific imaging features of MTM HCC. The results of this study revealed that MTM HCC exhibited more hypoenhancing components and early washout at CEUS than did non-MTM HCC. Like the results of previous studies, our results revealed the relationship of MTM HCC with higher serum AFP levels (≥100 ng/mL) and larger tumor size (11,16). We developed and validated a combined CEUS-clinical model using the four aforementioned features (early washout, hypoenhancing component, tumor size, and AFP level ≥ 100 ng/mL), enabling the noninvasive prediction of this HCC subtype. The model achieved AUCs of 0.89 and 0.81 in the training and validation cohorts, respectively, demonstrating high NPVs (94.2% and 88.0%, respectively) for MTM HCC. Of note, the model was associated with OS (HR: 2.26 [95% CI: 1.07, 4.79], $P = .03$).

This study revealed that tumor size and serum AFP levels were associated with MTM HCC, which is consistent with previous research (11,12). Elevated serum AFP levels are often associated with a large tumor size, advanced disease stage, and poor differentiation, all of which contribute to a less favorable prognosis (13). In clinical practice, the preoperative measurement of AFP levels can enhance confidence in diagnosing MTM HCC, whereas postoperative AFP monitoring may be more beneficial in detecting tumor recurrence among these patients than among those who are AFP-negative.

The hypoenhancing component observed at CEUS was associated with MTM HCC, in accordance with the biologic and molecular evidence related to this subtype (4,20). A large tumor size in MTM HCC is associated with neovascularization that predominantly develops around the periphery of the tumor, resulting in reduced perfusion and ischemia in the central region, leading to hypoenhancement (21,22). CEUS has a high sensitivity for vascular flow detection, suggesting that the degree of tumor perfusion could be detected and reflected in the sequence and degree of perfusion. Furthermore, previous studies revealed that predicted MTM HCCs express high levels of carbonic anhydrase IX, a specific indicator of a hypoxic microenvironment (23). This observation raises the possibility that the hypoenhancing

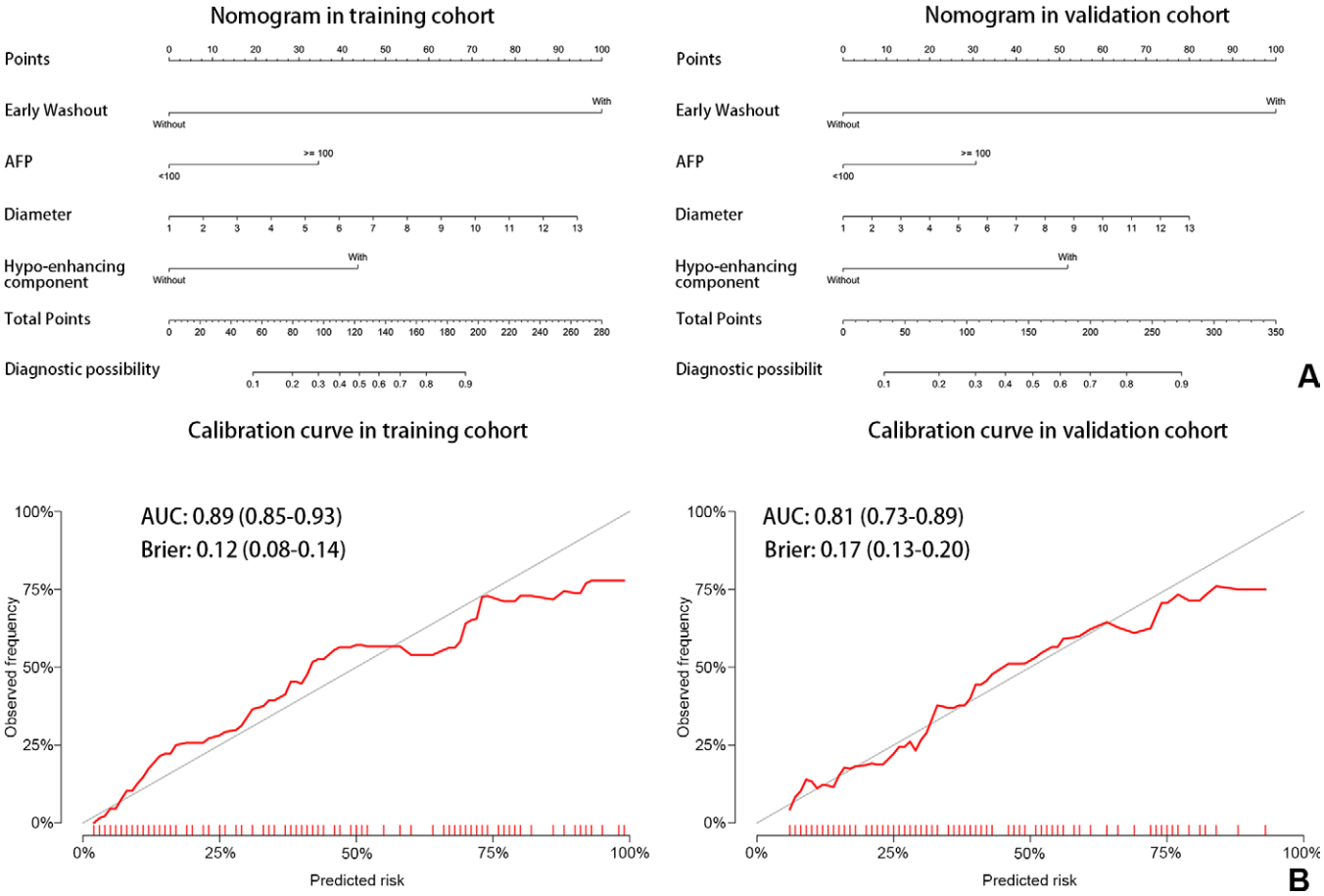

Figure 4: Development and validation of the MTM HCC prediction model. **(A)** Development and validation of MTM HCC predictive nomogram in training and validation cohorts. **(B)** Calibration curves in training and validation cohorts, which are well matched with the idealized 45° line in both cohorts. ***(Fig 4 continues)***

component may serve as a concrete manifestation of the hypoxic microenvironment. HCC is considered one of the most hypoxic solid cancers, contributing to treatment resistance and limiting long-term clinical benefits of systemic chemotherapy and immunotherapy. Combining standard therapies with inhibitors targeting hypoxia-related genes could represent a promising strategy for the treatment of patients with MTM HCC (24).

The findings of this study indicated a significant association between early washout and MTM HCC, which is considered a hallmark of hepatic malignancy (cholangiocarcinoma or liver metastasis), although not specifically for HCC. Some studies have reported that early washout is associated with poor differentiation and the aggressive biologic characteristics of HCCs (25,26), consistent with the proliferative nature of MTM HCC. Additionally, MTM HCC appears as a sinusoid-like microvasculature subtype, a microvascular pattern characterized by a continuous and branching vascular structure with an open sinusoidal space, occasionally referred as "vessels that encapsulate tumor clusters" (27). This subtype exhibits low microvascular density and a poor overall prognosis (28–31); the low microvascular density may be the reason for early washout at CEUS. HCCs with early washout at CEUS are more likely to have a high proportion of microvascular invasion, which corresponds to MTM HCC having a high proportion of microvascular invasion and poor prognosis. Patients with early-stage HCC categorized as LR-M have better postresection outcomes than those who undergo ablation (32). These findings may ultimately guide treatment decisions for patients with MTM HCC.

MTM HCC is also associated with posttreatment recurrence (33), and the predictive model developed in this study indicated that the high-risk group had worse OS and recurrence-free survival ($P < .001$ and .03, respectively) than those in the low-risk group. Furthermore, predicted MTM HCC was an independent predictor for OS. The prevalence of the MTM subtype in this study was 27.1% in the training cohort and 35.3% in the validation cohort, which are higher than the 16.0% prevalence reported by Ziol et al (7) but comparable to the 38.2% prevalence reported by Feng et al (11). This discrepancy might be associated with the cause, as MTM HCC is more likely to occur in individuals with HBV infection and large tumors (34), evidenced by the 80.9%–92.6% prevalence in the present study cohort as compared with 25.4% in that of Ziol et al's study (7).

Although previous studies have reported an association between necrosis and MTM HCC (9,11), we found no evidence of a difference in necrosis between the MTM and non-MTM HCC groups at CEUS in this study ($P > .05$). This finding is consistent with that of a previous study that used CEUS and conventional US to predict MTM HCC (17) and may be attributed to the high sensitivity of microbubbles at CEUS, in that even a very small amount of contrast agent perfusion can be detected.

The results of this study demonstrated a significant association between early washout and MTM HCC in lesions categorized as LR-M in patients with a high risk of HCC. A recent meta-analysis showed that patients with MTM HCC frequently show LR-M features at MRI, compared with those

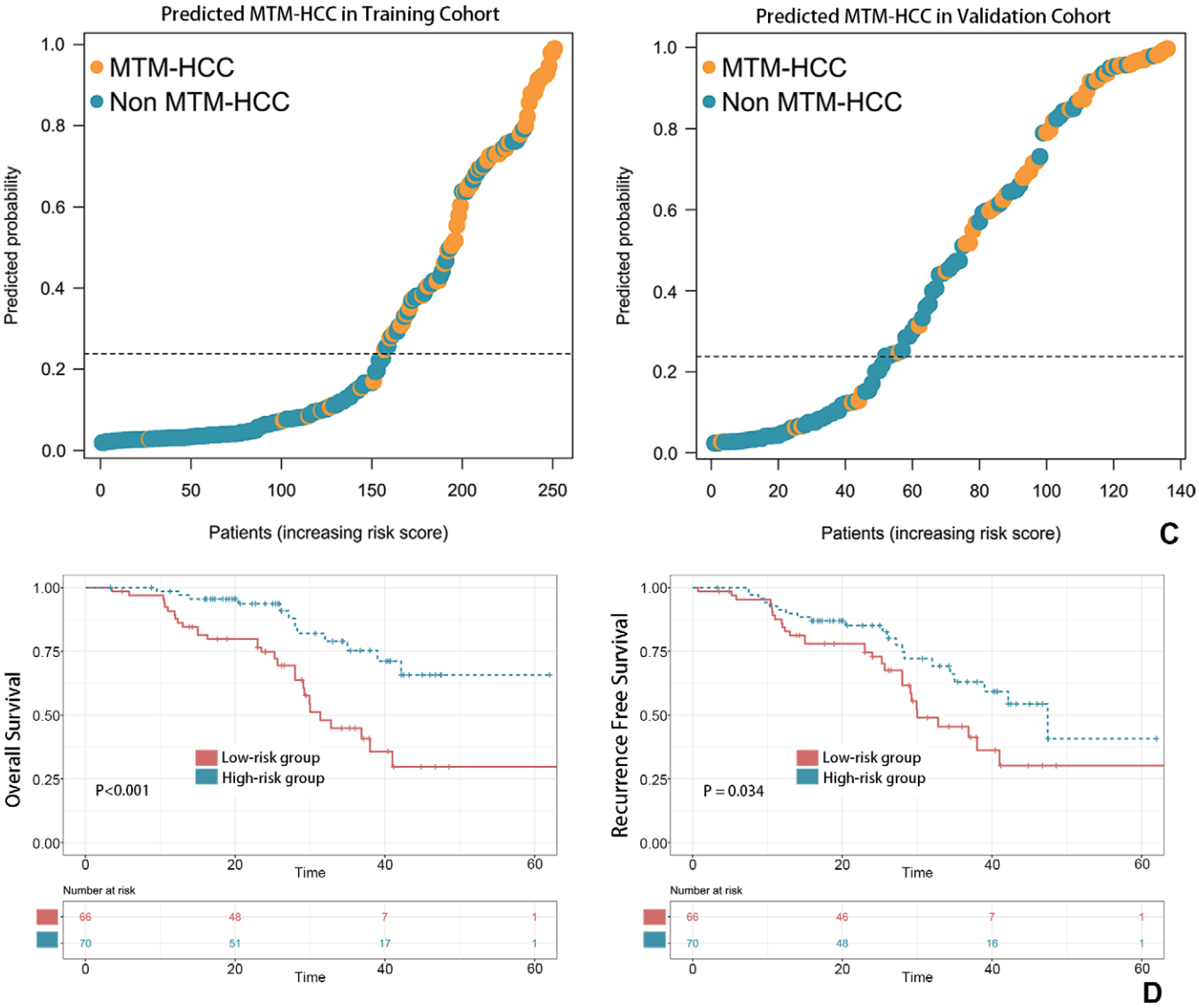

Figure 4 *(continued)*: **(C)** Risk distribution of predicted value of MTM HCC in training cohort and validation cohort; each dot represents a participant. The predicted risk probabilities are ranked from low to high, with the dotted line being the optimal cutoff value; the area above the dashed line is the model-predicted MTM HCC and below it is the model-predicted non-MTM HCC. The orange dots represent actual MTM HCC, and blue dots represent actual non-MTM HCC. **(D)** Kaplan-Meier curves stratified by the prediction model in the validation cohort show overall survival and recurrence-free survival. Time is measured in months. AFP = α-fetoprotein, AUC = area under the receiver operating characteristic curve, HCC = hepatocellular carcinoma, MTM = macrotrabecular massive.

with non-MTM HCCs (31). In accordance with Liver Imaging Reporting and Data System management, LR-M nodules in high-risk patients require biopsy or repeat imaging as LR-M indicates liver malignancy but not specifically HCC, meaning that MTM HCCs are more likely to require biopsy owing to their atypical imaging appearance. Previous studies have suggested that biopsies targeting the arterial phase enhancement region can avoid necrosis (35–37). The use of CEUS-guided biopsy for early washout and hypoenhancing components might improve the diagnostic accuracy of biopsy slides for MTM HCC, although this requires further clarification.

This study had some limitations. First, despite the inclusion of external cohort data, the retrospective nature of the study may have introduced selection bias. Additionally, as the primary cause was HBV infection, international validation is needed to increase the generalizability of our results. Second, although our results were based on MTM HCCs confirmed through resection, the results among the biopsy cohort were unclear; therefore, future studies should focus on patients who have undergone nonsurgical treatment after biopsy. Third, the quantitative analysis of CEUS might reflect the perfusion curve of tumors more precisely and facilitate the association between perfusion status and MTM HCC. Finally, the application of artificial intelligence–based approaches may help to enhance the efficacy of our predictive model and the exploration of further correlations between CEUS features and the angiogenesis of this cancer subtype.

Overall, the results of this study revealed that a combined CEUS-clinical model can be used to identify the MTM subtype of HCC, which was associated with poor patient outcomes. The ability to preoperatively recognize this subtype using this model could facilitate early risk stratification and guide closer surveillance strategies, especially for patients who undergo local therapy. Future studies should aim to validate this model in larger, multicenter cohorts and explore its integration with emerging biomarkers or radiogenomic data to further refine its predictive accuracy and clinical utility.

Table 4: Univariable and Multivariable Cox Regression Analysis for Overall Survival of Hepatocellular Carcinoma after Surgical Resection in the Validation Cohort

Clinical Characteristic	Univariable HR	*P* Value	Preoperative Multivariable HR	*P* Value
Sex (male vs female)	1.36 (0.29, 1.90)	.53	…	
Age	1.02 (0.96, 1.01)	.29	…	
Cause (non-HBV)	0.70 (0.22, 2.28)	.56	…	
Serum AFP level ≥ 100 ng/mL	1.96 (0.96, 3.69)	.07	…	
PLT count	1.00 (0.99, 1.01)	.13	…	
ALB level	0.91 (0.84, 0.98)	.02	0.90 (0.83, 0.98)	.01
TBIL level	1.01 (0.96, 1.08)	.63	…	
DBIL level	0.99 (0.89, 1.10)	.86	…	
Tumor size	1.23 (1.13, 1.35)	<.001	1.16 (1.06, 1.27)	.001
BCLC stage (B–C)	3.19 (1.71, 5.93)	<.001	…	
Multiple lesions	2.26 (1.18, 4.35)	.01	1.99 (1.00, 3.96)	.048
Predicted MTM HCC	4.02 (2.06, 7.81)	<.001	2.26 (1.07, 4.79)	.03

Note.—Data in parentheses are 95% CIs. Validation cohort consisted of 136 participants. AFP = α-fetoprotein, ALB = albumin, BCLC = Barcelona Clinic Liver Cancer, DBIL = direct bilirubin, HBV = hepatitis B virus, HR = hazard ratio, MTM = macrotrabecular massive, PLT = platelet, TBIL = total bilirubin.

Author affiliations:

[1] School of Medicine, Nankai University, Tianjin, China

[2] Department of Ultrasound, Fifth Medical Center of Chinese PLA General Hospital, Beijing, China

[3] The Second Medical Center & National Clinical Research Center for Geriatric Diseases, Department of Ultrasound, Chinese PLA General Hospital, Beijing, China

[4] Department of Interventional Ultrasound, First Medical Center of Chinese PLA General Hospital, No. 28 Fuxing Road, Beijing 100853, China

[5] Department of Medical Ultrasonics, Institute of Diagnostic and Interventional Ultrasound, The First Affiliated Hospital of Sun Yat-Sen University, Guangzhou, China

[6] Department of Pathology and Hepatology, The Fifth Medical Center of PLA General Hospital, National Clinical Research Center for Infectious Diseases, Beijing, China

[7] Department of Ultrasonography, Xiangya Hospital, Central South University, Changsha, China

Received October 31, 2024; revision requested December 11; revision received April 10, 2025; accepted May 30.

Address correspondence to: P.L. (email: liangping301@126.com).

Funding: This work was supported by the National Scientific Foundation Committee of China (grant nos. 82441011, 92159305, 82030047, 81627803, 82102076, and 91859201), the National Scientific Foundation Committee of Beijing (grant no. JQ18021), Military Fund for Geriatric Diseases (20BJZ42), Fostering Funds for National Distinguished Young Scholar Science Fund (2018-JQPY-002), the National Clinical Research Center for Geriatric Diseases (NCRCGPLAGH-2019011) of Chinese PLA General Hospital, and Chinese PLA General Hospital and Youth Autonomous Innovation Science Fund (22QNFC042).

Author contributions: Guarantors of integrity of entire study, **J.W., Sisi Liu, W.Z.D., Q.Z., Y.W., X.X., J.Z., J.Y., P.L.**; study concepts/study design or data acquisition or data analysis/interpretation, all authors; manuscript drafting or manuscript revision for important intellectual content, all authors; approval of final version of submitted manuscript, all authors; agrees to ensure any questions related to the work are appropriately resolved, all authors; literature research, **J.W., Sisi Liu, Y.Z., Q.Z., Y.W., X.Y., X.X., Shuhong Liu, J.Y., P.L.**; clinical studies, **J.W., Y.Z., W.Z.D., Q.Z., Y.W., F.X., X.Y., X.X., Shuhong Liu, J.Z., J.L., J.Y., P.L.**; statistical analysis, **J.W., Y.Z., Y.W., Shuhong Liu, P.L.**; and manuscript editing, **J.W., Sisi Liu, Y.Z., Y.W., X.Y., X.X., J.Y., P.L.**

Data sharing: All data generated or analyzed during the study are included in the published paper.

Disclosures of conflicts of interest: J.W. No relevant relationships. **Sisi Liu** No relevant relationships. **Y.Z.** No relevant relationships. **W.Z.D.** No relevant relationships. **Q.Z.** No relevant relationships. **Y.W.** No relevant relationships. **F.X.** No relevant relationships. **X.Y.** No relevant relationships. **X.X.** No relevant relationships. **Shuhong Liu** No relevant relationships. **J.Z.** No relevant relationships. **J.L.** No relevant relationships. **J.Y.** No relevant relationships. **P.L.** No relevant relationships.

References

1. Siegel RL, Miller KD, Fuchs HE, Jemal A. Cancer statistics, 2022. CA Cancer J Clin 2022;72(1):7–33.
2. Vogel A, Meyer T, Sapisochin G, Salem R, Saborowski A. Hepatocellular carcinoma. Lancet 2022;400(10360):1345–1362.
3. Yang JD, Hainaut P, Gores GJ, Amadou A, Plymoth A, Roberts LR. A global view of hepatocellular carcinoma: trends, risk, prevention and management. Nat Rev Gastroenterol Hepatol 2019;16(10):589–604.
4. Calderaro J, Ziol M, Paradis V, Zucman-Rossi J. Molecular and histological correlations in liver cancer. J Hepatol 2019;71(3):616–630.
5. Torbenson MS. Hepatocellular carcinoma: making sense of morphological heterogeneity, growth patterns, and subtypes. Hum Pathol 2021;112:86–101.
6. Torbenson MS, Ng IOL, Park YN, Roncalli M, Sakamoto M. WHO Classification of Tumours. World Health Organization, 2019.
7. Ziol M, Poté N, Amaddeo G, et al. Macrotrabecular-massive hepatocellular carcinoma: A distinctive histological subtype with clinical relevance. Hepatology 2018;68(1):103–112.
8. Jeon Y, Benedict M, Taddei T, Jain D, Zhang X. Macrotrabecular Hepatocellular Carcinoma: An Aggressive Subtype of Hepatocellular Carcinoma. Am J Surg Pathol 2019;43(7):943–948.
9. Mulé S, Galletto Pregliasco A, Tenenhaus A, et al. Multiphase Liver MRI for Identifying the Macrotrabecular-Massive Subtype of Hepatocellular Carcinoma. Radiology 2020;295(3):562–571.
10. Hruban R, Adsay N, Esposito I, et al. WHO Classification of Tumours Editorial Board: Digestive System Tumours. World Health Organization, 2019; 329–330.
11. Feng Z, Li H, Zhao H, et al. Preoperative CT for Characterization of Aggressive Macrotrabecular-Massive Subtype and Vessels That Encapsulate Tumor Clusters Pattern in Hepatocellular Carcinoma. Radiology 2021;300(1):219–229.
12. Feng Z, Li H, Liu Q, et al. CT Radiomics to Predict Macrotrabecular-Massive Subtype and Immune Status in Hepatocellular Carcinoma. Radiology 2023;307(1):e221291.
13. Reig M, Forner A, Rimola J, et al. BCLC strategy for prognosis prediction and treatment recommendation: The 2022 update. J Hepatol 2022;76(3):681–693.
14. Lin C, He Y, Liu M, et al. Vessels That Encapsulate Tumor Clusters (VETC) Predict cTACE Response in Hepatocellular Carcinoma. J Hepatocell Carcinoma 2023;10:383–397.
15. Woo HY, Rhee H, Yoo JE, et al. Lung and lymph node metastases from hepatocellular carcinoma: Comparison of pathological aspects. Liver Int 2022;42(1):199–209.
16. Rhee H, Cho ES, Nahm JH, et al. Gadoxetic acid-enhanced MRI of macrotrabecular-massive hepatocellular carcinoma and its prognostic implications. J Hepatol 2021;74(1):109–121.

17. Luo M, Liu X, Yong J, et al. Preoperative prediction of macrotrabecular-massive hepatocellular carcinoma based on B-Mode US and CEUS. Eur Radiol 2023;33(6):4024–4033.
18. CEUS LI-RADS® v2017 American College of Radiology Committee on LI-RADS® LI-RADS Assessment Categories. https://www.acr.org/-/media/ACR/Files/RADS/LI-RADS/CEUS-LI-RADS-2017-Essentials.pdf.
19. Calderaro J, Couchy G, Imbeaud S, et al. Histological subtypes of hepatocellular carcinoma are related to gene mutations and molecular tumour classification. J Hepatol 2017;67(4):727–738.
20. Calderaro J, Meunier L, Nguyen CT, et al. ESM1 as a Marker of Macrotrabecular-Massive Hepatocellular Carcinoma. Clin Cancer Res 2019;25(19):5859–5865.
21. Tohme S, Yazdani HO, Liu Y, et al. Hypoxia mediates mitochondrial biogenesis in hepatocellular carcinoma to promote tumor growth through HMGB1 and TLR9 interaction. Hepatology 2017;66(1):182–197.
22. Cannella R, Dioguardi Burgio M, Beaufrère A, et al. Imaging features of histological subtypes of hepatocellular carcinoma: Implication for LI-RADS. JHEP Rep 2021;3(6):100380.
23. Rhee H, An C, Kim HY, Yoo JE, Park YN, Kim MJ. Hepatocellular Carcinoma with Irregular Rim-Like Arterial Phase Hyperenhancement: More Aggressive Pathologic Features. Liver Cancer 2019;8(1):24–40.
24. Bao MHR, Wong CCL. Hypoxia, Metabolic Reprogramming, and Drug Resistance in Liver Cancer. Cells 2021;10(7):1715.
25. Cai WJ, Ying M, Zheng RQ, et al. Contrast-Enhanced Ultrasound Liver Imaging Reporting and Data System in Hepatocellular Carcinoma ≤5 cm: Biological Characteristics and Patient Outcomes. Liver Cancer 2023;12(4):356–371.
26. Jang HJ, Kim TK, Burns PN, Wilson SR. Enhancement patterns of hepatocellular carcinoma at contrast-enhanced US: comparison with histologic differentiation. Radiology 2007;244(3):898–906.
27. Fang JH, Xu L, Shang LR, et al. Vessels That Encapsulate Tumor Clusters (VETC) Pattern Is a Predictor of Sorafenib Benefit in Patients with Hepatocellular Carcinoma. Hepatology 2019;70(3):824–839.
28. Zou RH, Lin QG, Huang W, et al. Quantitative Contrast-Enhanced Ultrasonic Imaging Reflects Microvascularization in Hepatocellular Carcinoma and Prognosis after Resection. Ultrasound Med Biol 2015;41(10):2621–2630.
29. Murakami K, Kasajima A, Kawagishi N, Ohuchi N, Sasano H. Microvessel density in hepatocellular carcinoma: Prognostic significance and review of the previous published work. Hepatol Res 2015;45(12):1185–1194.
30. Zhang Q, Wu J, Bai X, Liang T. Evaluation of Intra-Tumoral Vascularization in Hepatocellular Carcinomas. Front Med (Lausanne) 2020;7:584250.
31. Kim TH, Woo S, Lee DH, Do RK, Chernyak V. MRI imaging features for predicting macrotrabecular-massive subtype hepatocellular carcinoma: a systematic review and meta-analysis. Eur Radiol 2024;34(10):6896–6907.
32. Hu YX, Yan CJ, Yun M, et al. Contrast-enhanced ultrasound liver imaging reporting and data system v2017: patient outcomes after treatment for early-stage hepatocellular carcinoma nodules with category 3-5 and category M. Br J Radiol 2023;96(1147):20220492.
33. Fang JH, Zhou HC, Zhang C, et al. A novel vascular pattern promotes metastasis of hepatocellular carcinoma in an epithelial-mesenchymal transition-independent manner. Hepatology 2015;62(2):452–465.
34. Rebouissou S, Nault JC. Advances in molecular classification and precision oncology in hepatocellular carcinoma. J Hepatol 2020;72(2):215–229.
35. Malone CD, Fetzer DT, Monsky WL, et al. Contrast-enhanced US for the Interventional Radiologist: Current and Emerging Applications. RadioGraphics 2020;40(2):562–588.
36. Wu W, Jing X, Xue GQ, et al. A Multicenter Randomized Controlled Study of Contrast-enhanced US versus US-guided Biopsy of Focal Liver Lesions. Radiology 2022;305(3):721–728.
37. Francica G, Meloni MF, de Sio I, et al. Biopsy of Liver Target Lesions under Contrast-Enhanced Ultrasound Guidance - A Multi-Center Study. Ultraschall Med 2018;39(4):448–453.